

A Little Bit More: Bitplane-Wise Bit-Depth Recovery

Abhijith Punnappurath and Michael S. Brown, *Member, IEEE*

Abstract—Imaging sensors digitize incoming scene light at a dynamic range of 10–12 bits (i.e., 1024–4096 tonal values). The sensor image is then processed onboard the camera and finally quantized to only 8 bits (i.e., 256 tonal values) to conform to prevailing encoding standards. There are a number of important applications, such as high-bit-depth displays and photo editing, where it is beneficial to recover the lost bit depth. Deep neural networks are effective at this bit-depth reconstruction task. Given the quantized low-bit-depth image as input, existing deep learning methods employ a single-shot approach that attempts to either (1) directly estimate the high-bit-depth image, or (2) directly estimate the residual between the high- and low-bit-depth images. In contrast, we propose a training and inference strategy that recovers the residual image bitplane-by-bitplane. Our bitplane-wise learning framework has the advantage of allowing for multiple levels of supervision during training and is able to obtain state-of-the-art results using a simple network architecture. We test our proposed method extensively on several image datasets and demonstrate an improvement from 0.5dB to 2.3dB PSNR over prior methods depending on the quantization level.

Index Terms—Bit depth, bitplane, quantization, image restoration

I. INTRODUCTION

THE term *bit depth* refers to the number of bits used per color channel to encode the tonal values of an image. Most modern camera sensors capture images with bit depths between 10 and 12 bits (representing 1024 and 4096 tonal values, respectively). The captured sensor image is then processed onboard the camera to transform it to a standard RGB (sRGB) image that is compatible with prevailing encoding standards [1]. The final step in the in-camera processing pipeline is to *quantize* the sRGB image into an 8-bit-per-channel format to match the bit depth of consumer displays and printers, the vast majority of which are 8 bit.

Bit-depth recovery is the task of recovering the bits lost due to quantization. An example is shown in Fig. 1. Bit-depth recovery has important applications in high-bit-depth (HBD) displays and photo editing. While most monitors are still 8 bit, 10-bit display devices are becoming increasingly popular due to ever-growing consumer demand for finer and more nuanced color tones. Many TVs, and smart phones such as Samsung Galaxy S10 [2] and iPhone X [3], already support 10-bit displays to meet high dynamic range (HDR) standards. However, these displays remain under-utilized as most image and video content available is still 8 bit. Artifacts are observed

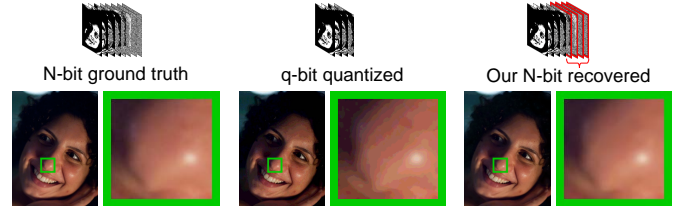


Fig. 1. The ground truth N -bit high-bit-depth (HBD) image, its q -bit quantized low-bit-depth (LBD) version, and our recovered N -bit HBD output are shown. Our proposed bit-depth recovery algorithm restores the q -bit quantized input image to its original bit depth of N by recovering the lost $(N-q)$ bits (shown in red), one bitplane at a time. The green box denotes a zoomed-in region of the image. While $(q, N)=(8, 10)$ or $(8, 12)$ are common target use cases in HBD displays or photo editing applications, most printers and monitors (and even this paper’s PDF format) are designed for 8-bit. Therefore, for the purpose of this example, we use $(q, N)=(4, 8)$ so that the quantization effects can be visually observed in print and on screen.

when 8-bit data is directly stretched to fit 10-bit monitors. Fig.2 shows the outputs obtained without and with bit-depth recovery applied as a pre-processing step. Note that HBD displays may further process the input (e.g., apply different rendering styles) to enhance the subjective quality and produce visually pleasing results. While displays often apply additional image enhancement operations, bit-depth recovery is fundamentally an image restoration task whose objective is to recover the actual bits lost due to quantization. Likewise, restoring the bit depth prior to photo editing reduces artifacts due to the availability of additional tonal values, as shown in Fig.2.

Several classical methods (e.g., [4], [5], [6], [7], [8], [9]) for bit-depth recovery exist in the literature. More recently, deep learning algorithms [10], [11], [12], [13], [14], [15], [16] have been proposed. The strategy employed by most deep learning methods (e.g., [10], [12], [13], [14], [15], [16]) is to train the network using the quantized low-bit-depth (LBD) image as input and have the network predict the high-bit-depth image as output. An alternative strategy recently proposed by Liu et al. [11] is to train the network to predict the residual between the ground truth HBD image and the quantized LBD image. At test time, this output residual image is added to the quantized LBD image to produce the desired HBD image. While these two strategies are equivalent, it is argued that from a deep neural network (DNN) training perspective, the latter is more efficient and provides faster convergence. We adopt this latter formulation in our work. However, as opposed to [11], who estimate the residual in a single shot, we propose to recover the residual image corresponding to the lost bits one bitplane

A. Punnappurath and M. S. Brown are with the Department of Electrical Engineering and Computer Science, York University, Toronto, Canada. E-mail: pabhijith@eecs.yorku.ca, mbrown@eecs.yorku.ca

Manuscript received April 19, 2005; revised August 26, 2015.

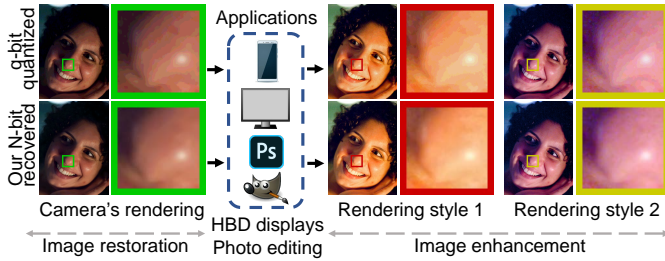


Fig. 2. An illustrative example demonstrating the importance of bit-depth recovery applied as a pre-processing step for HBD displays and photo editing applications. Stretching the quantized LBD image for display on an HBD device produces artifacts as can be seen from row one, whereas our recovered HBD image when provided as input leads to high-quality results as shown in row two. Photo editors too derive similar advantages from the availability of additional tonal values. Bit-depth recovery is a restoration task, and provides a canonical starting point for enhancement operations of choice applied during HBD display rendering or photo editing.

at a time.

Because the numerical magnitude of a pixel's tonal value decreases from the most significant bit to the least significant bit, the most significant bits dominate loss functions based on mean square error (MSE) or peak signal-to-noise ratio (PSNR). As a result, approaches that predict either the HBD image or the residual using single-shot training fail to capture the very fine details encoded by the lower-order bits. This observation is the impetus for our bitplane-wise training strategy that aims to overcome this limitation of existing methods.

Contributions Our proposed method is based on the observation that the residual between the high-bit-depth ground truth image and the quantized low-bit-depth input image can be expressed as a weighted summation of the bitplanes lost during quantization. Each bitplane is a binary map, and thus, the original task of predicting the residual can be reformulated into a series of better-constrained binary image segmentation problems. We train a separate neural network independently to predict each bitplane. This makes our method agnostic to the relative magnitude of the bit position, and overcome the limitation of the single-shot training strategy employed by existing approaches. The input images for training each network can be generated from the ground truth HBD image by applying the appropriate level of quantization. This multi-level-supervised training strategy outperforms state-of-the-art techniques using a simple network architecture. We compare our method against several classical as well as deep learning algorithms on five image datasets under a range of quantization levels and demonstrate that our method advances the state-of-the-art by a significant margin.

Scope We note that our method is focused strictly on bit-depth quantization and does not consider other strategies often used in bit-depth reduction, such as image halftoning [17], or color palette reduction, such as in GIF [18]. In addition, our method is not attempting inverse-tone mapping [19], [20], which is a technique for producing high-dynamic-range images from low-dynamic-range input images. While on the surface these appear as the same problem, the objectives of inverse-tone mapping and bit-depth recovery are different. Inverse tone

mapping is an image enhancement task that tries to maximize the *subjective* quality (this can include hallucinating details in under-/over-exposed regions) so that the result looks plausible on an HDR display. As previously mentioned, the aim of bit-depth recovery, and our algorithm in particular, is image restoration where the goal is to accurately recover the actual bits lost due to linear quantization.

II. RELATED WORK

Early work on bit-depth recovery was based on simple rules to fill the missing bits. Multiplication by an ideal gain is the most straightforward method, wherein the LBD image is simply multiplied by an ideal gain factor. Bit replication [4] fills the lost bits with copies of the current LBD bits. Although these methods are fast, they ignore the spatial characteristics of the image and produce visual artifacts. The minimum risk-based classification method [5] constructs prediction error histograms and assigns the value with the minimum associated risk as the HBD pixel intensity at that location. Interpolation-based methods [6], [7] have also been proposed. The contour region reconstruction algorithm [6] linearly interpolates pixel values by analyzing distances from upward contour edges and downward contour edges. A drawback of this method is that it fails in regions with local extrema. The content adaptive technique in [7] tackles this issue through the use of a virtual skeleton marking algorithm which converts the problematic 2D extrapolation in local extrema regions into simple 1D interpolation. Optimization-based approaches, such as [21], [8], are also popular. With this approach, the bit-depth recovery problem is formulated as a maximum a posteriori (MAP) estimation in [21]. The ACDC algorithm [8] applies graph signal processing to the bit-depth recovery task. The AC component of the desired HBD signal is first calculated using a MAP formulation, and the DC component is then computed using the AC estimate by applying a minimum MSE criterion. The IPAD technique [9] employs an intensity potential field to model the spatial correlation among the LBD pixels. The HBD image is recovered using a context-adaptive de-quantization procedure that leverages this potential field.

Recently, deep learning-based approaches have gained in popularity [10], [11], [12], [13], [14], [15], [16]. Works by Hou and Qiu [14] and GG-DCNN [15] employ a U-Net style architecture to predict the HBD image given the LBD image. Their methods aim to restore very low bit depth images (e.g., 2 bits). The networks of BE-CNN [10] and Liu et al. [16] comprise a chain of deconvolution layers with long and short skip connections. BitNet [12] uses an encoder-decoder architecture with dilated convolutions and multi-scale feature integration. BE-CALF [11] employs a chain of convolutional-deconvolutional layers with dense concatenations of all level features. BDEN [13] uses a two-stream architecture, one for flat and another for non-flat regions, with a local adaptive adjustment preprocessing step for the flat areas. Their approach is tailored towards relatively smaller expansions of the bit depth – 6 to 8 bit, 8 to 10 bit – while other methods [11], [10], [12] target larger expansions – 4 to 16 bit, 6 to 16 bit. Different deep learning methods use different loss functions to train their

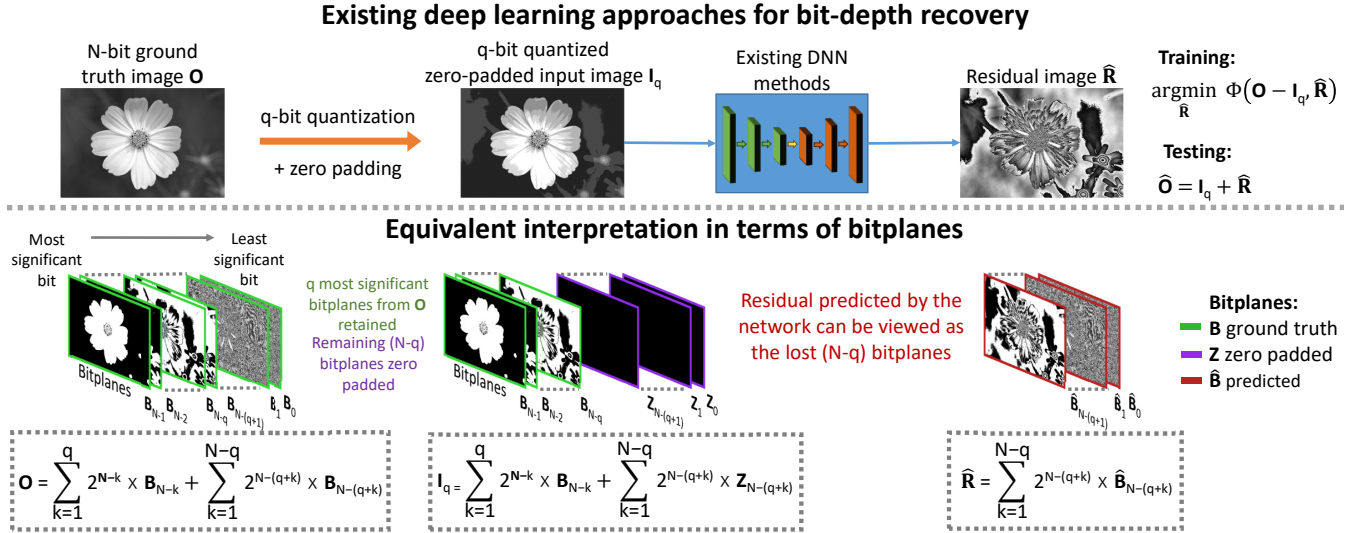


Fig. 3. Bit-depth recovery from a bitplane perspective. Existing DNN methods are trained to predict a residual image which when added to the input q -bit quantized LBD image produces the desired N -bit HBD output image. Interpreted as bitplanes, recovering the residual is equivalent to recovering the $(N-q)$ bitplanes lost during quantization. As opposed to existing methods that predict the full residual in a single shot, we propose to recover it one bitplane at a time using a multi-level-supervised training strategy.

models; MSE, mean absolute error (MAE), VGG features and so forth are the most common. It can be seen that existing deep learning methods resort to deeper and more complex architectures (U-Net style encoder-decoder, long-short skip connections, multi-stream networks, dense feature concatenations) to improve performance. In the following sections, we demonstrate how we can outperform these existing techniques across a variety of bit-depth ranges using a standard ResNet-style [22] network architecture. This is made possible by our bitplane-wise training strategy, explained in the following section.

III. PROPOSED METHOD

In this section, we first analyze the bit-depth recovery problem from a bitplane perspective. We then introduce our bitplane-wise training and testing strategy. Our network architecture is discussed in Sec. III-A.

Let the ground truth HBD image be denoted by \mathbf{O} . Assume \mathbf{O} has a bit depth of N . To quantize \mathbf{O} to q bits, the following formula can be applied [14], [15], [23]:

$$\mathbf{I}_q = \lfloor \frac{\mathbf{O}}{2^{(N-q)}} \rfloor 2^{(N-q)}, \quad (1)$$

where \mathbf{I}_q represents the q -bit quantized and zero padded LBD image, and $\lfloor \cdot \rfloor$ represents the `floor` operation. Existing deep learning algorithms, such as [10], [12], [13], [14], [15], [16], train using $(\mathbf{I}_q, \mathbf{O})$ pairs as input and target. We can also express \mathbf{O} as the summation of \mathbf{I}_q and a residual image \mathbf{R} :

$$\mathbf{O} = \mathbf{I}_q + \mathbf{R}. \quad (2)$$

Liu et al. [11] argue that training using $(\mathbf{I}_q, \mathbf{R})$ pairs as input and target yields better results. At test time, the estimate of the residual $\hat{\mathbf{R}}$ can simply be added to the input \mathbf{I}_q to generate the desired HBD image $\hat{\mathbf{O}}$. See row one of Fig. 3.

Our proposed method is based on the residual model in equation (2). In row two of Fig. 3, we present its equivalent interpretation in terms of bitplanes. The N -bit HBD ground truth image \mathbf{O} can be expressed as

$$\mathbf{O} = \sum_{k=1}^q 2^{N-k} \times \mathbf{B}_{N-k} + \sum_{k=1}^{N-q} 2^{N-(q+k)} \times \mathbf{B}_{N-(q+k)}, \quad (3)$$

where the first term corresponds to the q most significant bits and the second term corresponds to the $(N-q)$ least significant bits, and \mathbf{B} denotes a binary map of 0s and 1s. When \mathbf{O} is quantized to q bits using equation (1), we get

$$\mathbf{I}_q = \sum_{k=1}^q 2^{N-k} \times \mathbf{B}_{N-k} + \sum_{k=1}^{N-q} 2^{N-(q+k)} \times \mathbf{Z}_{N-(q+k)}, \quad (4)$$

where all entries of \mathbf{Z} are zero. The residual $\hat{\mathbf{R}}$ predicted by the network is thus

$$\hat{\mathbf{R}} = \sum_{k=1}^{N-q} 2^{N-(q+k)} \times \hat{\mathbf{B}}_{N-(q+k)}, \quad (5)$$

where $\hat{\mathbf{B}}$ is an estimate of the bitplanes. We use grayscale images in Fig. 3 for ease of visualization of the bitplanes – the extension to color images is straightforward.

Next, we describe in detail our training strategy. Given a q -bit quantized image \mathbf{I}_q , the objective is to recover the $(N-q)$ bitplanes $\hat{\mathbf{B}}$ lost during quantization, and restore \mathbf{I}_q to its original bit depth of N . Towards this goal, we train $(N-q)$ networks independently as shown in Fig. 4, where each network is trained to predict one single bitplane. Observe that \mathbf{I}_q retains q most significant bits from \mathbf{O} . Therefore, the first network labelled DNN $(q+1)$ is trained to predict the bitplane $N-(q+1)$. The input and target pairs for this network are the q -bit quantized image \mathbf{I}_q and the ground truth binary map $\mathbf{B}_{N-(q+1)}$, respectively, both of which can be obtained

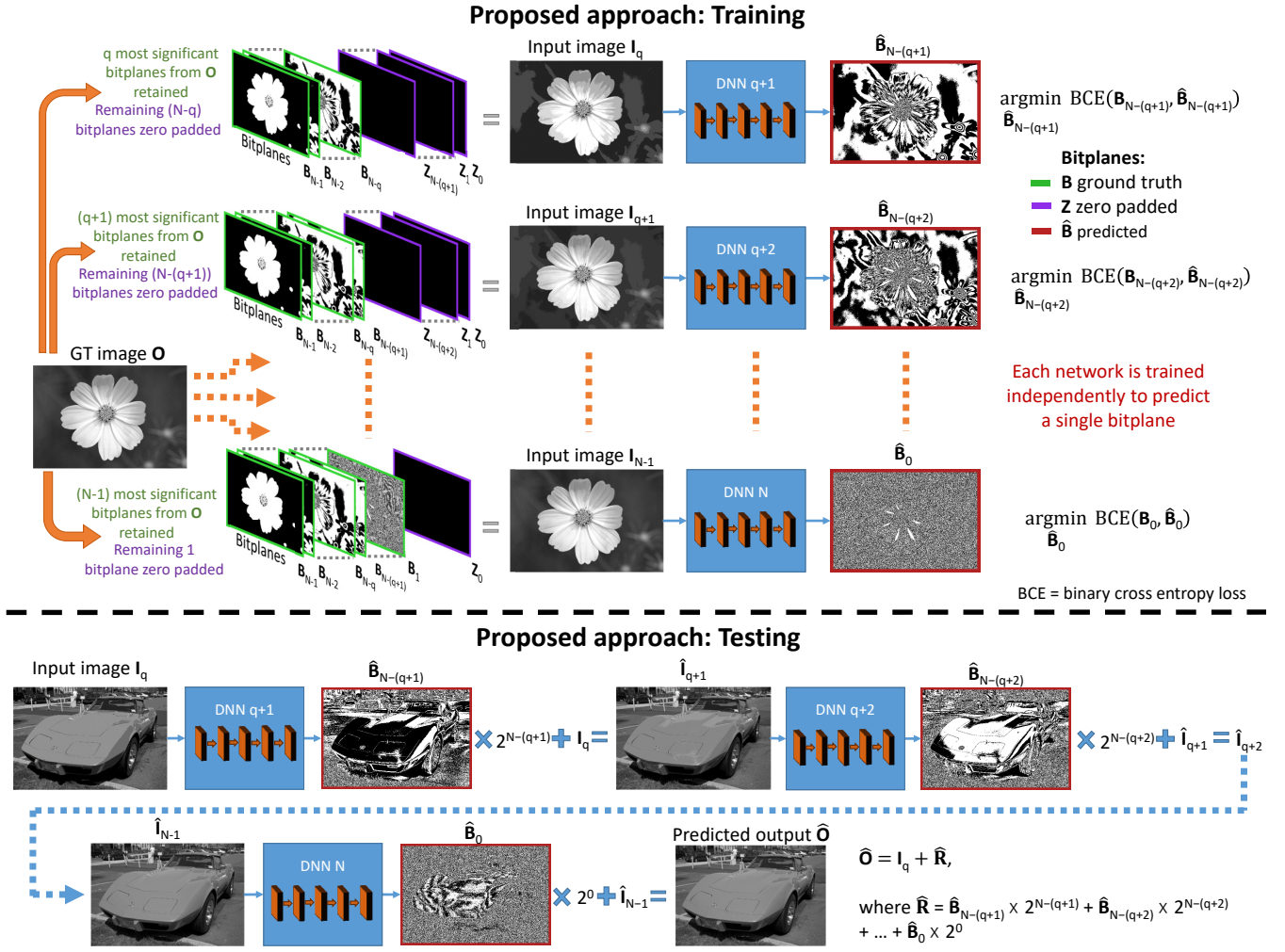


Fig. 4. Overview of our proposed approach. We train $(N-q)$ separate DNNs to recover the $(N-q)$ bitplanes lost during quantization. Here, N is the bit depth of the desired HBD image, and q the bit depth of the input LBD image. The input-target pairs $(\mathbf{I}_{q+k-1}, \mathbf{B}_{N-(q+k)})$, $k=1$ to $(N-q)$, for training each network can be computed directly from the HBD ground truth image \mathbf{O} . The target $\mathbf{B}_{N-(q+k)}$ is a binary map, and the problem reduces to one of binary image segmentation, which we optimize using a binary cross entropy loss. At test time, the q -bit quantized input LBD image \mathbf{I}_q is passed through the trained networks *sequentially*, with each network increasing the bit depth by one until the image is restored to its desired bit depth of N .

from the ground truth HBD image \mathbf{O} . We use the binary cross entropy (BCE) loss, which is typically applied to binary image segmentation problems, to train our network. The loss is computed between the ground truth binary map $\mathbf{B}_{N-(q+1)}$ and the network's prediction $\hat{\mathbf{B}}_{N-(q+1)}$.

In a similar manner, to predict the next least significant bit, we train DNN $(q+2)$ using the input-target pair $(\mathbf{I}_{q+1}, \mathbf{B}_{N-(q+2)})$, where \mathbf{I}_{q+1} is obtained by quantizing \mathbf{O} to $(q+1)$ bits using equation (1). This process is repeated for all $(N-q)$ bits – the last least significant bitplane is trained using DNN (N) with an $(N-1)$ -bit quantized image \mathbf{I}_{N-1} as input, and the ground truth binary map \mathbf{B}_0 as target. All our networks are trained using the same BCE loss as shown in Fig. 4.

At test time, the trained networks are applied sequentially as shown in Fig. 4. The q -bit quantized test image \mathbf{I}_q is first fed to DNN $(q+1)$. The network's prediction $\hat{\mathbf{B}}_{N-(q+1)}$ is multiplied by the appropriate weighting factor $2^{N-(q+1)}$ and this result is added to the input image \mathbf{I}_q to obtain our estimate

$\hat{\mathbf{I}}_{q+1}$. Note that at this stage, $\hat{\mathbf{I}}_{q+1}$, we have restored the q -bit quantized input \mathbf{I}_q to a bit depth of $(q+1)$. Next, we input this estimate $\hat{\mathbf{I}}_{q+1}$ to DNN $(q+2)$ to obtain its prediction $\hat{\mathbf{B}}_{N-(q+2)}$, which is multiplied by $2^{N-(q+2)}$ and added to $\hat{\mathbf{I}}_{q+1}$ to obtain our $(q+2)$ -bit-depth estimate, $\hat{\mathbf{I}}_{q+2}$. Repeating this process till the last bit produces our estimate of the HBD image $\hat{\mathbf{O}}$.

A. Network architecture

Our network architecture is shown in Fig. 5. The input is a 3-channel RGB image \mathbf{I}_{q+k-1} . The network predicts a 3-channel output $\hat{\mathbf{B}}_{N-(q+k)}$ having the same size as the input. Here, k is the index that runs over the bitplanes – namely, $k=1$ to $(N-q)$. We use the same architecture for all $(N-q)$ bitplanes. As previously mentioned, each of these $(N-q)$ networks is trained independently. Our architecture consists of an initial convolution layer (Conv), a series of D residual blocks, followed by a batch normalization (BN) layer and a

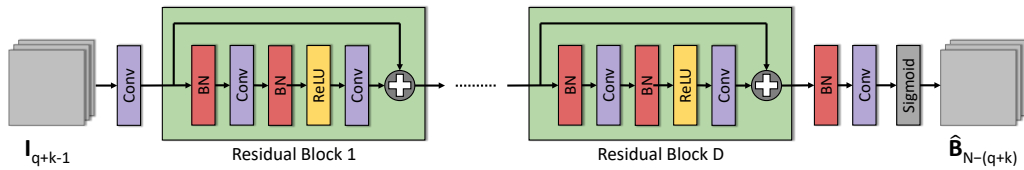


Fig. 5. A diagram of our network architecture. We train $(N-q)$ networks, one for each bitplane lost during quantization. Compared to existing DNN architectures for bit-depth recovery that use encoder-decoder modules, dense feature concatenation layers, multiple streams, and more, our architecture is a standard ResNet-style [22] structure with a series of residual blocks. Even with just four residual blocks (i.e., $D=4$), we can achieve state-of-the-art results based on our bitplane-wise training framework.

TABLE I
RESULTS ON SINTEL DATASET [24]. THE BEST RESULTS ARE REPORTED IN BOLD AND RED. THE SECOND, THIRD, AND FOURTH BEST-PERFORMING METHODS ARE SHOWN IN GREEN, BLUE, AND YELLOW, RESPECTIVELY.

		ZP	MIG	BR [4]	MRC [5]	CRR [6]	CA [7]	ACDC [8]	IPAD [9]	BE-CNN [10]	BE-CALF [11]	Ours D4	Ours D16
4-16 bit	PSNR	28.7692	31.9004	32.4604	33.7792	33.7982	35.5001	34.6394	35.7647	36.3070	39.8474	40.9274	41.5070
	SSIM	0.8843	0.8826	0.8947	0.9126	0.9348	0.9436	0.9077	0.9451	0.9486	0.9612	0.9786	0.9810
4-12 bit	PSNR	28.7916	31.9140	32.4655	33.7915	33.8342	35.5171	34.6384	35.7753	36.3071	39.8478	40.9286	41.5080
	SSIM	0.8844	0.8827	0.8948	0.9126	0.9352	0.9438	0.9077	0.9452	0.9485	0.9611	0.9786	0.9810
4-8 bit	PSNR	29.1599	32.1404	32.6690	33.9525	34.3592	35.7051	34.5944	35.8610	36.2505	39.7621	40.6143	41.1909
	SSIM	0.8864	0.8847	0.8989	0.9141	0.9389	0.9444	0.9074	0.9457	0.9446	0.9565	0.9773	0.9794
6-16 bit	PSNR	40.8072	44.2780	44.4131	46.8504	46.0178	46.9613	46.6553	47.6154	49.7405	51.1430	52.7599	53.4825
	SSIM	0.9857	0.9858	0.9862	0.9903	0.9864	0.9896	0.9858	0.9902	0.9926	0.9940	0.9976	0.9979
6-12 bit	PSNR	40.9029	44.3357	44.4725	46.8886	46.1370	47.0376	46.6522	47.6593	49.7421	51.1454	52.7491	53.4731
	SSIM	0.9858	0.9858	0.9864	0.9903	0.9867	0.9898	0.9858	0.9903	0.9926	0.9940	0.9976	0.9980

final convolution layer. The last layer is a sigmoid activation restricting all pixel values to lie in the range $[0,1]$. Our residual blocks are styled after [13] and contain two convolution layers, two batch normalization layers, and a rectified linear unit (ReLU). There is an additive skip connection between the input and output of each residual block. All convolution filters are of size 3×3 and padded such that the input and output are of the same size. We use a fixed number of 64 filters for all convolution layers. The depth of our network is determined primarily by the number of residual units D . As we shall demonstrate in Sec. IV, we can already outperform all competing approaches with $D=4$. We also experiment with $D=16$ and show that this gives up a further boost in performance.

We note that our primary focus is *not* the choice of network architecture, but rather to evaluate the effectiveness of our bitplane-wise training strategy for bit-depth recovery. Other

recent works have used more complex architectures, such as dense feature concatenations, multiple streams, and encoder-decoder structures. While such configurations are indeed possible, our aim is to demonstrate that a standard ResNet-style [22] architecture can produce state-of-the-art results with bitplane-wise training. We would also like to add that while our architecture resembles a single stream of BDEN [13], their overall network structure is more complex with two streams and a local adaptive adjustment preprocessing step applied to one stream.

Our method requires us to train separate models for each bitplane. While this may be seen as cumbersome, competing methods, such as [13], [14], also train separate models depending on the bit depth of the quantized input image.

IV. RESULTS

In this section, we first provide details regarding how we train our networks. Next, we evaluate the performance of our algorithm against competing approaches both quantitatively and qualitatively using five publicly available image datasets.

A. Training

We use 2000 color images, 1000 each from the Sintel dataset [24] and the MIT-Adobe FiveK dataset [25], for training. Sintel is a short animation film, and the dataset contains more than 20,000 16-bit lossless images at a resolution of 436×1024 pixels. Following [11], [10], we select 1000 images at random from this dataset. The MIT-Adobe FiveK dataset is a natural image dataset consisting of 5000 images in raw format captured using different SLR cameras covering a broad range

TABLE II
RESULTS ON MIT-ADOBE FIVEK DATASET [25].

		ZP	MIG	BR [4]	IPAD [9]	BitNet [12]	Ours D4	Ours D16
3-16 bit	PSNR	22.8986	25.2658	26.4256	29.8615	33.4260	33.7891	34.1088
	SSIM	0.7381	0.7334	0.7817	0.8624	0.9086	0.9252	0.9279
4-16 bit	PSNR	28.8587	31.7121	32.2720	35.7357	38.6340	39.6484	39.9478
	SSIM	0.8769	0.8745	0.8876	0.9378	0.9587	0.9683	0.9693
5-16 bit	PSNR	34.8596	37.9655	38.2413	41.1847	43.4240	44.8035	44.9396
	SSIM	0.9556	0.9554	0.9580	0.9743	0.9826	0.9871	0.9876
6-16 bit	PSNR	40.8795	44.1029	44.2380	46.4284	48.2250	49.5657	49.7193
	SSIM	0.9871	0.9872	0.9876	0.9903	0.9935	0.9951	0.9953

TABLE III
RESULTS ON TESTIMAGES 1200 DATASET [26].

		ZP	MIG	BR [4]	MRC [5]	CRR [6]	CA [7]	ACDC [8]	IPAD [9]	BE-CNN [10]	BE-CALF [11]	Ours D4	Ours D16
4-16 bit	PSNR	28.8322	31.5393	32.0988	34.2227	33.5094	35.1968	34.7447	36.1890	32.3203	38.5099	39.6503	40.4099
	SSIM	0.8739	0.8711	0.8845	0.9169	0.9243	0.9343	0.8994	0.9443	0.9443	0.9658	0.9700	0.9735
4-12 bit	PSNR	28.8543	31.5545	32.0993	34.2385	33.5428	35.2121	34.7422	36.2000	32.3191	38.5095	39.6619	40.4216
	SSIM	0.8741	0.8712	0.8847	0.9170	0.9247	0.9344	0.8993	0.9444	0.9442	0.9657	0.9700	0.9735
4-8 bit	PSNR	29.2192	31.8072	32.2102	34.4698	34.0535	35.3879	34.6727	36.2924	32.2774	38.4572	39.6822	40.3906
	SSIM	0.8764	0.8736	0.8896	0.9175	0.9295	0.9354	0.8986	0.9450	0.9426	0.9640	0.9691	0.9725
6-16 bit	PSNR	40.8621	43.8101	43.9437	47.0584	45.3877	45.2110	46.7708	47.1574	46.9513	49.8488	51.5413	52.1203
	SSIM	0.9855	0.9856	0.9861	0.9912	0.9852	0.9881	0.9871	0.9899	0.9924	0.9945	0.9964	0.9967
6-12 bit	PSNR	40.9570	43.8747	43.9823	47.0986	45.5076	45.2845	46.7661	47.2052	46.9528	49.8521	51.5490	52.1220
	SSIM	0.9856	0.9857	0.9863	0.9912	0.9856	0.9883	0.9871	0.9901	0.9924	0.9945	0.9964	0.9967

TABLE IV
RESULTS ON KODAK DATASET [27]. NR DENOTES THAT A SCORE WAS ‘NOT REPORTED’ IN THE ORIGINAL PAPER.

		ZP	MIG	BR [4]	MRC [5]	CRR [6]	CA [7]	ACDC [8]	IPAD [9]	BitNet [12]	BE-CALF [11]	Ours D4	Ours D16
3-8 bit	PSNR	22.7767	25.8250	27.0293	28.3804	28.2246	29.1447	28.6566	29.2012	32.6830	NR	33.5089	33.6679
	SSIM	0.7671	0.7604	0.8036	0.8246	0.8304	0.8413	0.8200	0.8515	0.9181	NR	0.9319	0.9337
4-8 bit	PSNR	29.0657	32.6293	33.3027	35.2607	34.1294	34.7382	34.6817	34.9081	38.4820	38.9392	39.4171	39.5185
	SSIM	0.8998	0.8969	0.9108	0.9270	0.9293	0.9317	0.9152	0.9345	0.9657	0.9680	0.9709	0.9723

TABLE V
RESULTS ON ESPL V2 DATASET [28].

		ZP	MIG	BR [4]	MRC [5]	CRR [6]	CA [7]	ACDC [8]	IPAD [9]	BE-CNN [10]	BitNet [12]	Ours D4	Ours D16
3-8 bit	PSNR	23.2092	25.4391	26.6110	27.3040	26.9249	29.4643	28.6803	29.8653	NR	32.8760	33.0186	33.3581
	SSIM	0.6616	0.6571	0.7242	0.7381	0.7990	0.8245	0.7764	0.8379	NR	0.8802	0.8949	0.8971
4-8 bit	PSNR	29.2893	31.8492	32.4288	34.2636	34.2817	35.7807	34.6381	35.7558	35.4100	38.9680	39.1687	39.3012
	SSIM	0.8261	0.8240	0.8453	0.8763	0.9046	0.9184	0.8818	0.9207	0.9400	0.9459	0.9513	0.9509

of scenes, subjects, and lighting conditions. Each raw image has been retouched in Adobe Lightroom by five professionals, and these five variations, saved as 16-bit lossless TIFF files, are available as part of the dataset. We use the first 1000 images (i.e., filenames a0001 to a1000) enhanced by a random expert for training. To ensure that images across both datasets are roughly the same resolution, all images from the MIT-Adobe dataset are downsampled by a factor of 4. While some papers [13], [14], [15], [12] use natural images for training, others [11], [10] argue that animated images represent harder examples, and are thus more appropriate. In our experiments, we found that a balanced mix of animated and natural images gives the best generalization.

For training, we crop non-overlapping patches of size 48×48 pixels from all 2000 images. Data augmentation is performed by randomly flipping the patches, or rotating them by 90° . We use the Adam optimizer [29] with a learning rate of 10^{-3} and a batch size of 128. The learning rate is divided by 5 after 16 epochs. All our models are trained for 30 epochs using these same settings. We implemented our method using TensorFlow [30]. Our code and corresponding pre-trained models are publicly available at <https://github.com/abhijithpunnappurath/a-little-bit-more>.

B. Evaluation

We compare our proposed method against eight classical (i.e., non-deep learning) algorithms – (1) zero padding (ZP), (2) multiplication by ideal gain (MIG), (3) bit replication (BR) [4], (4) minimum risk-based classification (MRC) [5], (5) contour region reconstruction (CRR) [6], (6) content-adaptive image bit-depth enhancement (CA) [7], (7) maximum a posteriori estimation of AC signal (ACDC) [8], and (8) intensity potential for image de-quantization (IPAD) [9]. We also compare against three recent deep learning methods – (1) concatenating all level features (BE-CALF) [11], (2) learning-based bit-depth expansion (BitNet) [12], and (3) bit-depth enhancement with CNN (BE-CNN) [10]. The codes of the eight classical algorithms are implemented in Matlab¹ by the authors of [9]. In the case of the deep learning methods [11], [12], [10], the pre-trained models/codes are not publicly available. Therefore, for fair comparison, we report our scores on the same datasets using the same quantization levels that these papers have reported their results on. For all experiments in this section, the scores of the deep learning methods are copied directly from the original papers. Moreover, different papers have used different datasets for testing. To facilitate

¹<https://sites.google.com/site/jingliu198810/publication>

comparisons against all methods, we evaluate the performance of our method on three natural image datasets – MIT-Adobe FiveK [25], TESTIMAGES [26], and Kodak [27] – and two animated image datasets – Sintel [24] and ESPL v2 [28]. For quantitative evaluation, PSNR (dB) and structural similarity index (SSIM) [31] are chosen as metrics.

BE-CALF [11] and BE-CNN [10] have used the Sintel dataset [24] to report results. Following [11], [10], we select 50 random images (different from the training set) from this dataset for evaluation. Table I shows the scores of our proposed algorithm as well as various competing methods, including BE-CALF and BE-CNN, on these images. Two variants of our proposed method corresponding to two different network depths are tested – D4 and D16, corresponding to $D=4$ and $D=16$ residual units, respectively, as explained in Sec. III-A. The best results are reported in bold and red. The second, third, and fourth best-performing methods are shown in green, blue, and yellow, respectively. Both [11] and [10] are trained exclusively on animated images from Sintel while we use a mix of natural and animated images for training. Yet, as can be seen from the results, both our models outperform BE-CALF and BE-CNN by a sound margin across all quantization levels.

BitNet [12] has used the last 1000 images (i.e., filenames a4001 to a5000) of the MIT-Adobe dataset [25] enhanced by expert E for testing. The scores on these images are reported in Table S4. Note that BitNet is trained exclusively on the first 4000 images enhanced by expert E, while we use only 1000 images by a random expert. Once again, it can be observed from the results that both our models outperform all comparison techniques, including BitNet.

The remaining three datasets, TESTIMAGES [26], Kodak [27], and ESPL v2 [28], are not part of our training set. We evaluate our method’s generalizability by testing on these images. The TESTIMAGES dataset [26] contains 40 1200×1200 16-bit natural images. The scores are reported in Table III. The Kodak dataset [27] is a natural image dataset consisting of 24 768×512 images with a bit depth of 8. The results on this dataset are reported in Table IV. ESPL v2 [28] contains 25 1920×1080 animated images also with a bit depth of 8. Following [12], we used only the pristine images without any distortion, and the scores are presented in Table V. It can be seen from the results in Tables III, IV, and V that our method outperforms all competing algorithms on both animated and natural images across a diversity of bit depths and image resolutions, thereby validating the effectiveness of our bitplane-wise training strategy.

Qualitative results are shown in Fig. 6. Unfortunately, the output images from the prior deep learning papers’ PDFs ([11], [12], [10]) are not high quality, and so we do not use them for qualitative evaluation. Our qualitative comparisons in Fig. 6 are restricted to the eight classical non-deep-learning methods. Following prior literature [12], [10], [13], we use only images with a maximum bit depth of 8 for qualitative evaluation such that they are suitable for display on standard 8-bit monitors. In the first example, it can be observed that all comparison methods have artifacts either along the horizontal bars or in the top right corner of the image. In the second result shown, the outputs of CRR [6] and CA [7] have smoothed out the

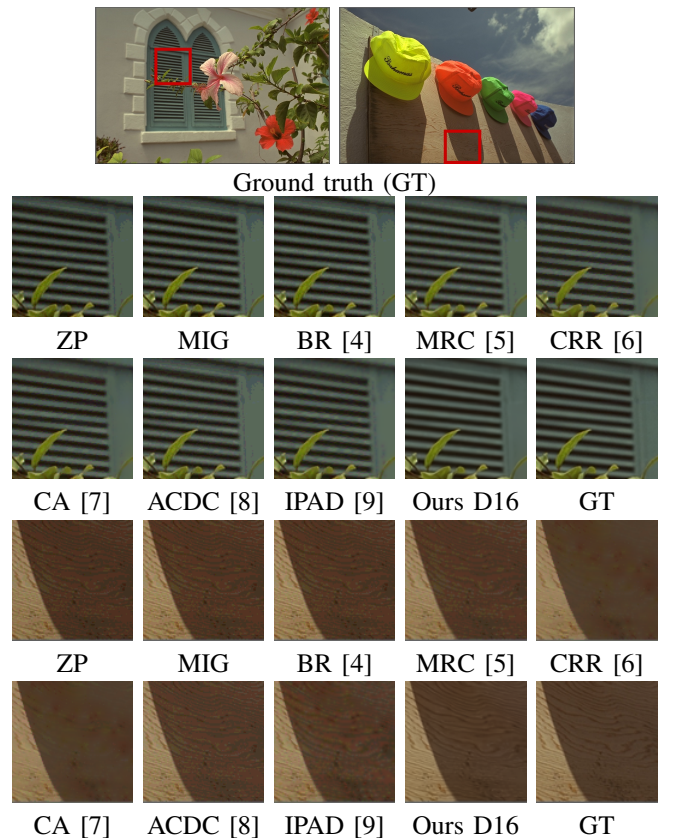


Fig. 6. Qualitative comparisons on the Kodak dataset for 4 to 8 bit recovery.

fine details, while all other competing algorithms have visible artifacts in the textured regions. In comparison, our results more closely match the ground truth in both cases, with most of the fine details restored and hardly any noticeable artifacts. Additional results are provided in the supplementary.

Accuracy versus model size: The plot of Fig. 7 shows the PSNR (dB) versus number of model parameters on the Kodak dataset for the 4-8 bit scenario (see Table IV). Our method is compared against BE-CALF [11], our closest competitor, and BitNet [12], which is the next best-performing method. Our D4 model has approximately 1.2 million parameters in total while D16 requires 4.77 million to recover 4 bitplanes. In comparison, BE-CALF, at 5.18 million parameters, is roughly four times bigger than D4 while yielding a PSNR about half a dB lower than our models. While BitNet has roughly the same

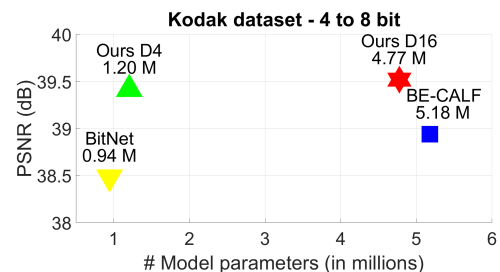


Fig. 7. PSNR (dB) versus number of model parameters.

TABLE VI
TESTIMAGES 1200 DATASET [26] FOR 4 TO 8-BIT RECOVERY, WITH $D=16$. PERFORMANCE IMPROVES AS EACH LOST BITPLANE (FROM 5 TO 8) IS RECOVERED.

Bitplane accumulated	5th	6th	7th	8th
PSNR (dB)	34.5088	38.5677	40.1036	40.3906
SSIM	0.9520	0.9694	0.9723	0.9725

model size as our D4 variant, its PSNR is approximately 1 dB lower than D4.

Single-shot baseline comparison: Our proposed method employs $(N-q)$ networks with D residual blocks each. For comparison, we trained a single network with the same total capacity by stacking together $(N-q) \times D$ residual blocks. The network was trained (under identical settings) to directly predict the residual using an MSE loss, with the final sigmoid layer removed. On the TESTIMAGES 1200 dataset [26], for example, for $D=4$, $N=8$, and $q=4$, the single-shot model obtained PSNR/SSIM values of 37.4822/0.9665, while our proposed method produced values of 39.6822/0.9691 (see Table III). This demonstrates the advantages of our bitplane-wise training strategy over the single-shot approach.

Accumulating bitplanes: Table VI shows that there is a performance gain as each lost bitplane is incrementally restored, and serves as an indicator of the effectiveness of bitplane-wise training.

Running time: On a 3.10 GHz processor with 32 GB RAM and an NVIDIA GeForce GTX 1080 GPU, our D4 model takes approximately 0.09 seconds per bitplane to process a 768×512 resolution image, while our D16 model takes 0.31 seconds on average. Since the pre-trained models/codes of competing DNN methods are unavailable, we cannot provide a fair comparison of running time by testing on the same hardware configuration. The running times of the classical methods are reported in the supplementary.

V. CONCLUSION

We have proposed a new DNN training strategy for bit-depth recovery where the residual image corresponding to the bits lost due to quantization is recovered bitplane by bitplane. Bitplane-wise learning makes our method independent of the relative magnitude of the bit position, overcoming the limitation of existing single-shot approaches. Experiments on five benchmark datasets demonstrate that our method outperforms the state of the art by up to 2.3 dB PSNR depending on the quantization level. As future work, we plan to explore the sharing of features across bitplanes instead of training networks completely independent of each other. We also plan to examine bitplane-wise training for other residual estimation problems.

REFERENCES

- [1] H. C. Karaimer and M. S. Brown, "A software platform for manipulating the camera imaging pipeline," in *ECCV*, 2016.
- [2] [Online] <https://www.samsung.com/global/galaxy/galaxy-s10/specs/>.
- [3] [Online] https://support.apple.com/kb/sp770?locale=en_US.
- [4] R. A. Ulichney and S. Cheung, "Pixel bit-depth increase by bit replication," in *Color Imaging: Device-Independent Color, Color Hardcopy, and Graphic Arts*. SPIE, 1998.
- [5] G. Mittal, V. Jakhethiya, S. Jaiswal, O. Au, A. Tiwari, and W. Dei, "Bit-depth expansion using minimum risk based classification," in *Visual Communications and Image Processing*, 2012.
- [6] C. Cheng, O. Au, C. H. Liu, and K. Yip, "Bit-depth expansion by contour region reconstruction," in *IEEE International Symposium on Circuits and Systems*, 2009.
- [7] P. Wan, O. Au, K. Tang, Y. Guo, and L. Fang, "From 2D extrapolation to 1D interpolation: Content adaptive image bit-depth expansion," in *IEEE International Conference on Multimedia and Expo*, 2012.
- [8] P. Wan, G. Cheung, D. Florencio, C. Zhang, and O. Au, "Image bit-depth enhancement via maximum a posteriori estimation of AC signal," *IEEE Transactions on Image Processing*, vol. 25, no. 6, pp. 2896–2909, 2016.
- [9] J. Liu, G. Zhai, X. Yang, and C.-W. Chen, "IPAD: Intensity potential for adaptive de-quantization," *IEEE Transactions on Image Processing*, vol. 27, no. 10, pp. 4860–4872, 2018.
- [10] Y. Su, W. Sun, J. Liu, G. Zhai, and P. Jing, "Photo-realistic image bit-depth enhancement via residual transposed convolutional neural network," *Neurocomputing*, 2019.
- [11] J. Liu, W. Sun, Y. Su, P. Jing, and X. Yang, "BE-CALF: Bit-depth enhancement by concatenating all level features of DNN," *IEEE Transactions on Image Processing*, vol. 28, no. 10, pp. 4926–4940, 2019.
- [12] J. Byun, K. Shim, and C. Kim, "BitNet: Learning-based bit-depth expansion," in *ACCV*, 2019.
- [13] Y. Zhao, R. Wang, W. Jia, W. Zuo, X. Liu, and W. Gao, "Deep reconstruction of least significant bits for bit-depth expansion," *IEEE Transactions on Image Processing*, vol. 28, no. 6, pp. 2847–2859, 2019.
- [14] X. Hou and G. Qiu, "Image companding and inverse halftoning using deep convolutional neural networks," *arXiv*, 2017.
- [15] Y. Xiao, C. Pan, Y. Zheng, X. Zhu, Z. Qin, and J. Yuan, "Gradient-guided DCNN for inverse halftoning and image expanding," in *ACCV*, 2019.
- [16] J. Liu, W. Sun, and Y. Liu, "Bit-depth enhancement via convolutional neural network," in *Digital TV and Wireless Multimedia Communication*, 2018.
- [17] G. Sharma, *Digital Color Imaging Handbook*. CRC Press, Inc., 2002.
- [18] "Graphics interchange format, version 89a," [Online] <https://www.w3.org/Graphics/GIF/spec-gif89a.txt>.
- [19] G. Eilertsen, J. Kronander, G. Denes, R. K. Mantiuk, and J. Unger, "HDR image reconstruction from a single exposure using deep CNNs," *ACM Transactions on Graphics*, vol. 36, no. 6, pp. 1–15, 2017.
- [20] S. Y. Kim, J. Oh, and M. Kim, "Deep SR-ITM: Joint learning of super-resolution and inverse tone-mapping for 4K UHD HDR applications," in *ICCV*, 2019.
- [21] M. Ikebe and A. Mizuno, "Bit-depth expansion for noisy contour reduction in natural images," in *ICASSP*, 2016.
- [22] K. He, X. Zhang, S. Ren, and J. Sun, "Deep residual learning for image recognition," in *CVPR*, 2016.
- [23] Y. Li, L. Sharan, and E. H. Adelson, "Compressing and companding high dynamic range images with subband architectures," *ACM Transactions on Graphics*, vol. 24, no. 3, pp. 836–844, 2005.
- [24] Xiph Foundation, "xiph.org," [Online]. Available: <http://www.xiph.org/>.
- [25] V. Bychkovsky, S. Paris, E. Chan, and F. Durand, "Learning photographic global tonal adjustment with a database of input / output image pairs," in *CVPR*, 2011.
- [26] N. Asuni and A. Giachetti, "TESTIMAGES: A large-scale archive for testing visual devices and basic image processing algorithms," in *Smart Tools and Apps for Graphics Conference*, 2014.
- [27] Eastman Kodak, "Kodak lossless true color image suite," 1999, [Online]. Available: <http://r0k.us/graphics/kodak/>.
- [28] D. Kundu and B. Evans, "Full-reference visual quality assessment for synthetic images: A subjective study," in *ICIP*, 2015.
- [29] D. Kingma and J. Ba, "Adam: A method for stochastic optimization," *ICLR*, 2014.
- [30] M. et. al., "TensorFlow: Large-scale machine learning on heterogeneous systems," 2015. [Online]. Available: <https://www.tensorflow.org/>
- [31] Z. Wang, A. Bovik, H. Sheikh, and E. Simoncelli, "Image quality assessment: From error visibility to structural similarity," *IEEE Transactions on Image Processing*, vol. 13, no. 4, pp. 600–612, 2004.
- [32] T. L. et. al., "Microsoft COCO: Common objects in context," *arXiv*, 2014. [Online]. Available: <http://arxiv.org/abs/1405.0312>
- [33] D. Martin, C. Fowlkes, D. Tal, and J. Malik, "A database of human segmented natural images and its application to evaluating segmentation algorithms and measuring ecological statistics," in *ICCV*, 2001.
- [34] E. Agustsson and R. Timofte, "NTIRE 2017 challenge on single image super-resolution: Dataset and study," *CVPR Workshop*, 2017.

Supplementary Material

This supplementary material provides additional results and details that could not be included in the main paper due to space constraints. Ablation studies on our network architecture are presented in Sec. S1. In Secs. S2 and S3, we provide further quantitative and qualitative comparisons and results. The running times of various methods are reported in Sec. S4. An example highlighting the importance of bit-depth recovery for photo editing is furnished in Sec. S5.

S1. ABLATION STUDIES FOR DIFFERENT D VALUES

We performed ablation studies by varying the number of residual units D in our network architecture (see Fig. 5 of our main paper). Specifically, we tested the following values $D = 2, 4, 8, 12, 16, 20$. The average PSNR (dB) and SSIM versus D on the TESTIMAGES 1200 dataset [26] are shown in the plots of Fig. S1. We have reported results, both in the main paper and this supplementary, for our D4 and D16 variants. We have showed that we already outperform existing methods with $D = 4$. Beyond $D = 16$, we did not observe an improvement in performance.

S2. ADDITIONAL QUANTITATIVE RESULTS

We compare against the deep learning methods of Hou et al. [14] and GG-DCNN [15], who have trained and tested their models on the Microsoft COCO [32] dataset. Their pre-trained models/codes are not available. Following GG-DCNN [15], we use 2000 random images from the testing fold of this dataset. The authors of [15] have re-implemented the method of [14], and in Table S1, the results of both [15] and [14] are copied from [15]. Note that [15] report results on downsampled images of size 256×256 and 512×512 (in line with their training settings). We reproduce the best scores of [15] and [14] in Table S1. Also, since resizing to square images in this manner alters the aspect ratio, the results of our method are reported on the original-sized images. It can

be observed from the results in Table S1 that our PSNR values are significantly higher than [14] and [15].

The TESTIMAGES dataset [26] contains 40 16-bit natural images. While [11], [10] have reported results on the 1200×1200 resolution variant of this dataset, BitNet [12] has used 800×800 resolution images. We reported comparisons with [11], [10] in Table 3 of our main paper on 1200×1200 resolution images. In Table S2 of this supplementary, we present comparisons with BitNet [12] on 800×800 resolution images. (Following [12], we used image files with the shifting indicator ‘B01C00’.) From the results, it can be observed that both our models, D4 and D16, outperform BitNet on both metrics.

In Table S3, we report results for 8 to 10 bit, and 8 to 12 bit recovery on the Sintel dataset [24] and TESTIMAGES dataset [26]. The vast majority of high-bit-depth (HBD) monitors available today are 10 bit, and therefore, 8 to 10 bit reconstruction represents the most common scenario of bit-depth recovery applied to high-bit-depth displays. Modern camera sensors have a dynamic range of 10–12 bits. Thus, 8 to 12 bit recovery is the typical range for photo editing applications. Competing deep neural network (DNN) methods have not provided their results for these quantization levels. Since their pre-trained models/codes are not publicly available, their values are not reported in Table S3. It can be seen that our proposed method obtains higher accuracy than competing classical approaches. Results on MIT-Adobe FiveK dataset [25] for the same quantization levels are provided in Table S4. Comparisons against CRR [6], CA [7], and ACDC [8] have been omitted since there are 1000 images in the test set, and the running times (see Table S6) of these methods are very high. Moreover, from Tables 1 to 5 of the main paper, and Table S2 of the supplementary material, it can be observed that IPAD [9], on average, performs the best among the classical methods, and the results of this method have been included in Table S4. Our method outperforms IPAD [9] and other competitors, such as MRC [5], by a sound margin.

BDEN [13] has reported scores on the Kodak dataset [27] and the BSD100 dataset for 6 to 8 bit recovery. The BSD100 dataset consists of 100 images selected from the Berkeley Segmentation dataset [33]. A demo version of the code for the

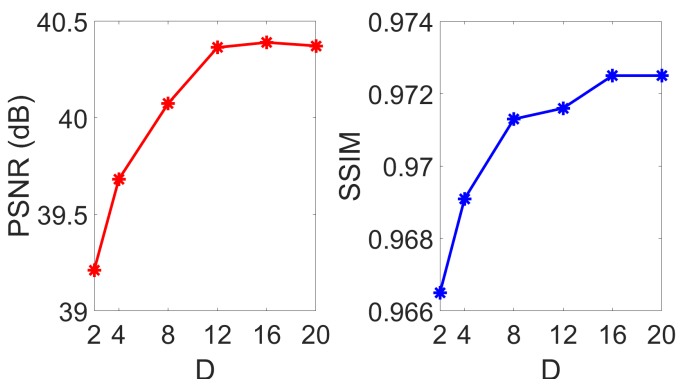


Fig. S1. PSNR (dB) and SSIM versus number of residual units D in our network architecture on the TESTIMAGES 1200 dataset [26].

TABLE S1

RESULTS ON MICROSOFT COCO DATASET [32]. FOLLOWING THE CONVENTION USED IN THE MAIN PAPER, THE BEST RESULTS ARE REPORTED IN BOLD AND RED. THE SECOND, THIRD, AND FOURTH BEST-PERFORMING METHODS ARE SHOWN IN GREEN, BLUE, AND YELLOW, RESPECTIVELY. NR DENOTES THAT A SCORE WAS ‘NOT REPORTED’ IN THE ORIGINAL PAPER.

	Hou [14]	GG-DCNN [15]	Ours D4	Ours D16
4-8 bit PSNR	35.8800	37.5300	39.4171	39.4344
SSIM	NR	NR	0.9625	0.9629

TABLE S2
RESULTS ON TESTIMAGES 800 DATASET [26].

		ZP	MIG	BR	MRC	CRR	CA	ACDC	IPAD	BitNet	Ours D4	Ours D16
3-16 bit	PSNR	22.7573	25.2648	26.4243	27.5546	26.4007	28.8859	28.8005	29.4943	32.5980	32.9752	33.4297
	SSIM	0.7550	0.7508	0.7965	0.8212	0.8393	0.8612	0.8199	0.8739	0.9069	0.9237	0.9291
4-16 bit	PSNR	28.8342	31.5370	32.0966	34.3637	33.2068	34.8206	34.7631	35.5728	38.9560	39.3081	40.0830
	SSIM	0.8846	0.8822	0.8946	0.9233	0.9237	0.9336	0.9086	0.9417	0.9630	0.9699	0.9734
5-16 bit	PSNR	34.8447	37.6917	37.9665	40.7613	39.3272	40.1733	40.7694	41.1885	44.4810	45.1050	45.8028
	SSIM	0.9574	0.9571	0.9597	0.9727	0.9670	0.9717	0.9649	0.9749	0.9857	0.9890	0.9903
6-16 bit	PSNR	40.8653	43.8044	43.9379	46.9165	45.0570	45.0097	46.7881	46.6101	49.4040	50.6359	51.0936
	SSIM	0.9872	0.9873	0.9877	0.9918	0.9863	0.9887	0.9889	0.9902	0.9948	0.9964	0.9966

TABLE S3
8-10 BIT AND 8-12 BIT RECOVERY.

		ZP	MIG	BR	MRC	CRR	CA	ACDC	IPAD	Ours D4	Ours D16
Results on Sintel dataset [24]											
8-10 bit	PSNR	54.6856	57.2202	56.3490	59.5132	58.3145	58.2976	58.2234	58.4633	60.8031	60.9087
	SSIM	0.9991	0.9991	0.9991	0.9993	0.9991	0.9992	0.9989	0.9993	0.9997	0.9997
8-12 bit	PSNR	53.2583	56.6246	56.4774	59.4131	57.7446	58.1010	58.6677	58.7444	62.9363	63.2755
	SSIM	0.9990	0.9990	0.9990	0.9993	0.9984	0.9989	0.9989	0.9990	0.9997	0.9998
Results on TESTIMAGES 1200 dataset [26]											
8-10 bit	PSNR	54.7353	56.8199	55.5634	59.3286	57.9548	55.9924	58.3119	57.9176	59.9239	60.0357
	SSIM	0.9992	0.9991	0.9991	0.9993	0.9991	0.9991	0.9992	0.9992	0.9996	0.9996
8-12 bit	PSNR	53.3181	56.1645	55.9193	59.1269	57.2560	55.6482	58.7748	57.9785	61.2724	61.5413
	SSIM	0.9990	0.9990	0.9990	0.9993	0.9985	0.9988	0.9991	0.9989	0.9996	0.9996
Results on TESTIMAGES 800 dataset [26]											
8-10 bit	PSNR	54.7371	56.8124	55.5558	59.1069	57.9243	56.6157	58.3242	57.7774	59.3925	59.4411
	SSIM	0.9993	0.9993	0.9992	0.9994	0.9992	0.9992	0.9992	0.9993	0.9996	0.9996
8-12 bit	PSNR	53.3218	56.1560	55.9105	58.9844	57.2802	56.2646	58.7920	57.8165	60.4816	60.6476
	SSIM	0.9991	0.9992	0.9992	0.9994	0.9987	0.9989	0.9992	0.9991	0.9996	0.9996

deep learning method in BDEN has been publicly released by the authors [13]. However, it works only on grayscale images, and the model has been trained using only the first 100 images from the DIV2K [34] dataset, while their actual model in the paper is trained on color images using all 800 images from this dataset. In consideration of these limitations, for fair comparison, we directly copy results reported in their paper instead of running their demo code. The results are presented in Table S5. We would like to note that our bitplane-wise recovery strategy offers the most advantage over single-shot methods for larger expansions of the bit depth e.g., 8-12 bit, 6-12 bit etc. In the present case, the expansion is only 2 bits (from 6 to 8), and hence, our PSNR values are only slightly higher than BDEN.

S3. ADDITIONAL QUALITATIVE RESULTS

Qualitative comparisons for 4 to 8 bit recovery on Kodak [27], MIT-Adobe FiveK [25], and Sintel [24] datasets are provided in Figs. S2, S3, and S4, respectively. Zoomed-in patches are presented for better visualization. Furthermore, regions of interest are marked with a circle on the zoomed-in ground truth patch in Figs. S3, and S4. Representative structures including smooth color transitions, edges, and fine textures are shown. As already mentioned in the main paper, our qualitative comparisons are limited to the eight classical

TABLE S4
RESULTS ON MIT-ADOBE FIVEK DATASET [25].

		ZP	MIG	BR	MRC	IPAD	Ours D4	Ours D16
8-10 bit	PSNR	54.7390	57.0704	56.2218	57.5123	57.6648	58.8890	58.8877
	SSIM	0.9993	0.9992	0.9992	0.9992	0.9992	0.9995	0.9995
8-12 bit	PSNR	53.3305	56.4642	56.3202	58.7387	57.7665	59.7254	59.7783
	SSIM	0.9992	0.9992	0.9992	0.9994	0.9991	0.9995	0.9995

methods since the pre-trained models/codes of competing DNN methods are unavailable.

In the first example of Fig. S2, the thin line structures on the sail of the boat have been smoothed out in the outputs of CRR [6] and CA [7], while all other comparison methods have artifacts in the gray region on the top left. In comparison, our method recovers the fine lines on the sail and produces very few artifacts. In the second example of Fig. S2, artifacts are visible in the region below the eye in the results of all comparison algorithms except CRR. The output of CRR is overly smooth and lacks detail. The texture in this region is much better recovered in our outputs.

In the two examples of Fig. S3, it can be seen that the structure in the clouds (see in particular the region marked by the circle on the ground truth patch) is best reconstructed in our outputs with our D16 model performing visually better than our D4 model. Fig. S4 shows two cases with fine texture,

TABLE S5
6–8 BIT RECOVERY.

		ZP	MIG	BR	MRC	CRR	CA	IPAD	B DEN	Ours D16
BSD100 [33]	PSNR	41.1397	43.0056	42.6987	43.9878	43.2519	43.3038	43.1991	47.7800	48.1065
	SSIM	0.9898	0.9896	0.9896	0.9915	0.9909	0.9910	0.9911	NR	0.9967
Kodak [27]	PSNR	42.5077	45.5028	45.1540	47.1685	45.5719	45.7344	45.5074	47.7900	47.8255
	SSIM	0.9918	0.9915	0.9915	0.9929	0.9917	0.9918	0.9915	NR	0.9953

TABLE S6
AVERAGE RUNNING TIMES OF DIFFERENT ALGORITHMS ON THE KODAK DATASET [27] FOR 4 TO 8 BIT RECOVERY.

Method	ZP	MIG	BR [4]	MRC [5]	CRR [6]	CA [7]	ACDC [8]	IPAD [9]	Ours D4	Ours D16
Time (s)	0.0063	0.0023	0.0035	0.6411	318.86	397.51	1457.40	39.14	0.36	1.24

with the second example being particularly challenging. In the second example, it can be seen from the results that all competing methods fail completely in recovering the fine strands in the region enclosed by the white circle. In contrast, these details are clearly visible in our outputs and very closely match the ground truth.

outputs. This example highlights the importance of bit-depth recovery for photo editing.

S4. RUNNING TIME

In Table S6, we report the average running times of the eight classical methods on the Kodak dataset [27] which contains images of size 768×512 pixels. The 4 to 8 bit recovery scenario is tested. As already mentioned in the main paper, we used the codes made publicly available by the authors of [9] to compare against these classical methods. The implementations are CPU-based. In the last two columns of Table S6, the average running times of our D4 and D16 models to process four bitplanes are reported. Our method is implemented on GPU. Although ZP, MIG, and BR [4] are extremely fast, their performance is poor. CRR [6], CA [7], and ACDC [8] have high computational complexity, and their outputs are inferior to ours both qualitatively and quantitatively. Although the difference in the testing environment (CPU versus GPU) biases a direct comparison of running times in our favour, it is still noteworthy that our proposed method is much faster than IPAD, which is the best performing classical method. More importantly, our method produces more accurate results than IPAD.

S5. PHOTO EDITING APPLICATION

The ability to edit an image post-capture can be adversely affected by quantization to 8 bits. Fig. S5-(A) shows a common example of a captured 8-bit sRGB image having low contrast. Applying a simple histogram equalization operation on this 8-bit image to enhance its contrast produces the undesired “stair-step” effect shown in Fig. S5-(B). This artifact is a direct consequence of the quantization process whereby tonal information was lost. Fig. S5-(B) shows the results of histogram equalization when applied to the original unquantized 12-bit image (which is usually unavailable) and our recovered 12-bit result. Due to the additional tonal values in the 12-bit histograms, the banding artifacts are not present in these

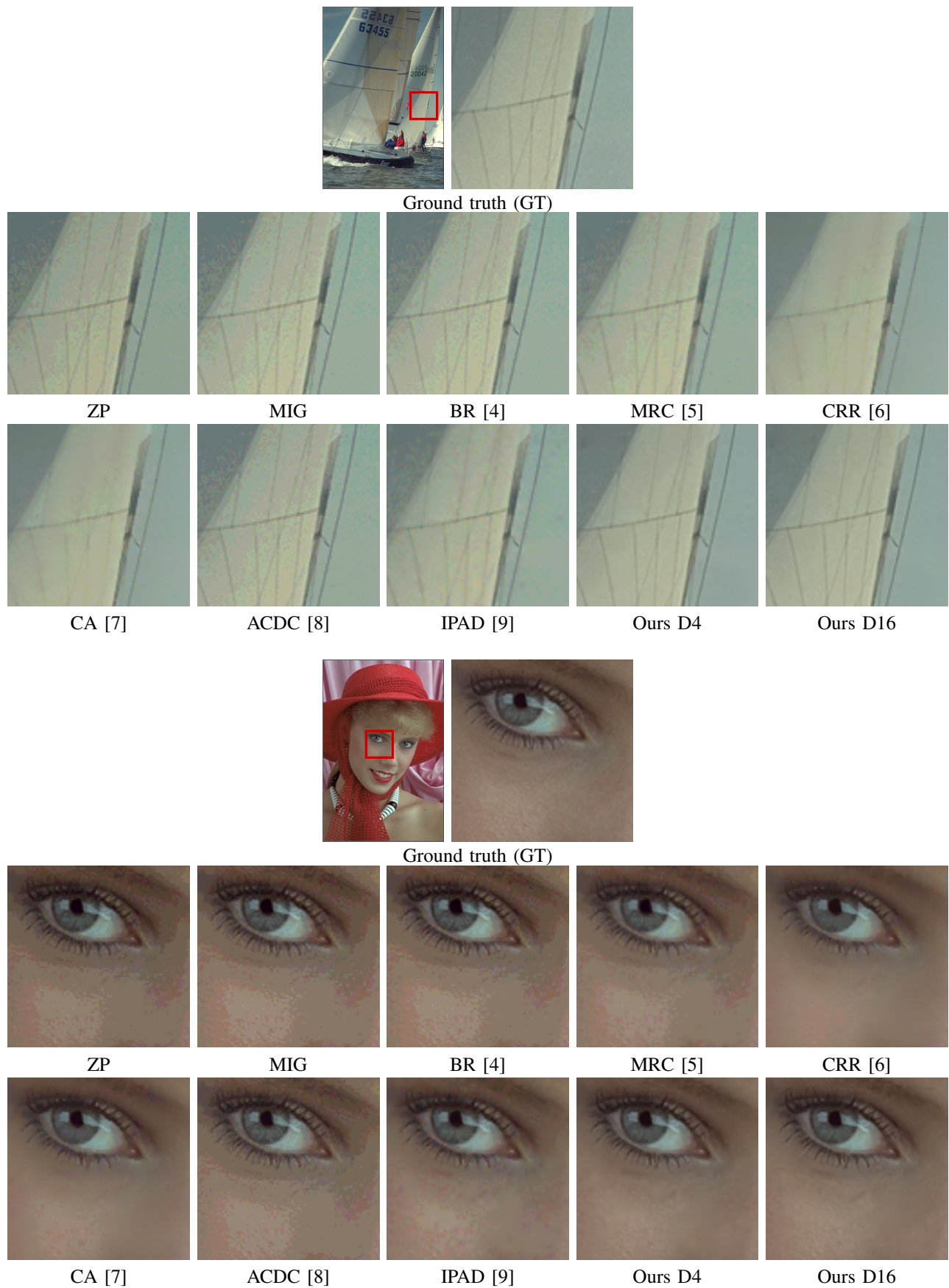


Fig. S2. Qualitative comparisons on the Kodak dataset [27] for 4 to 8 bit recovery.

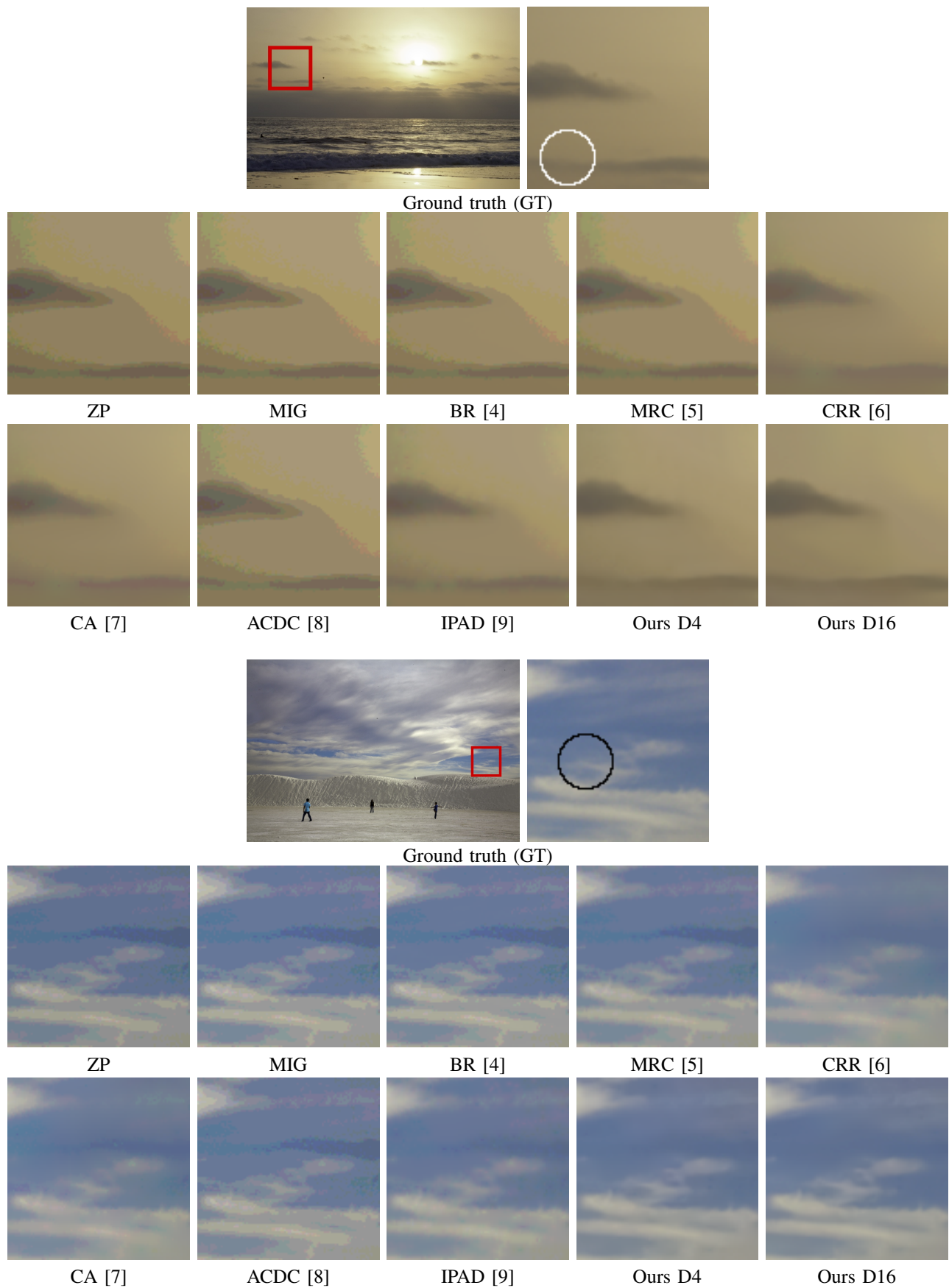


Fig. S3. Qualitative comparisons on the MIT-Adobe FiveK dataset [25] for 4 to 8 bit recovery.

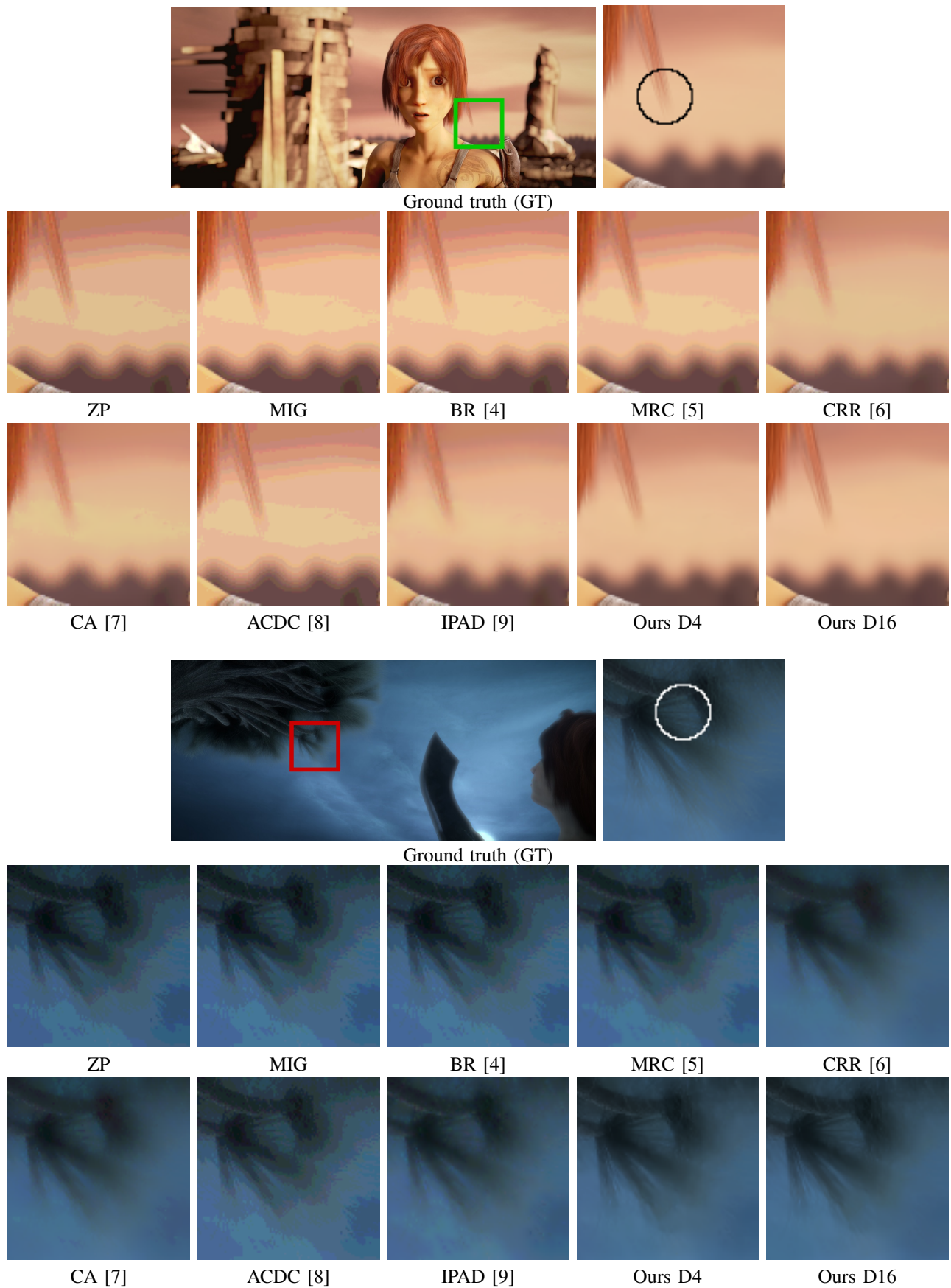
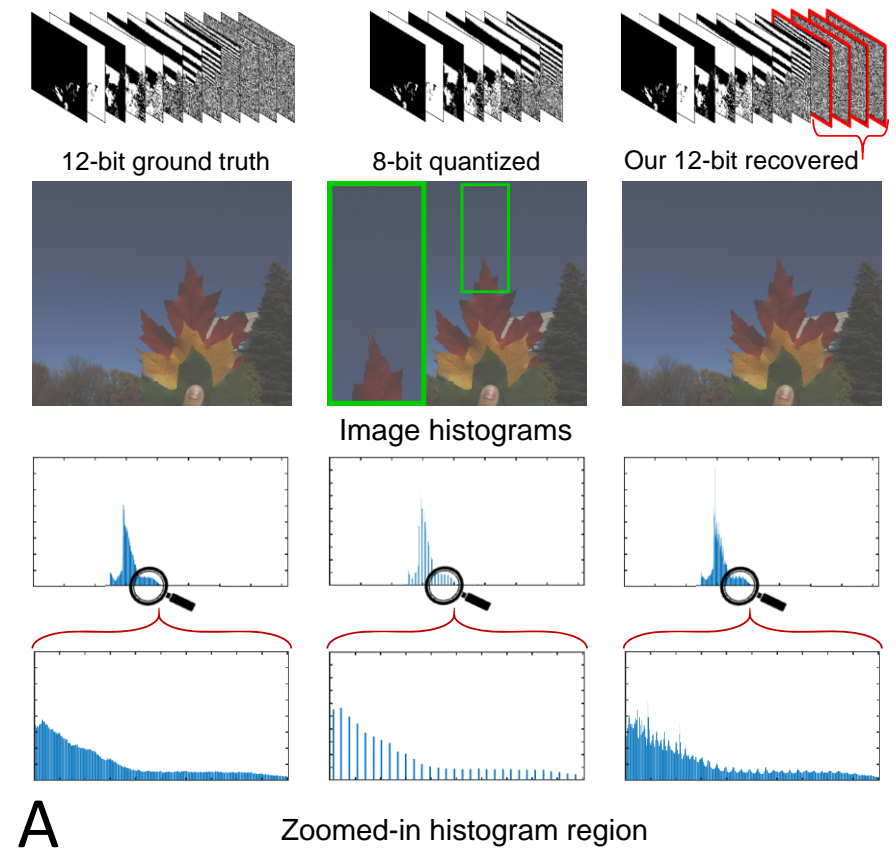


Fig. S4. Qualitative comparisons on the Sintel dataset [24] for 4 to 8 bit recovery.



After histogram equalization

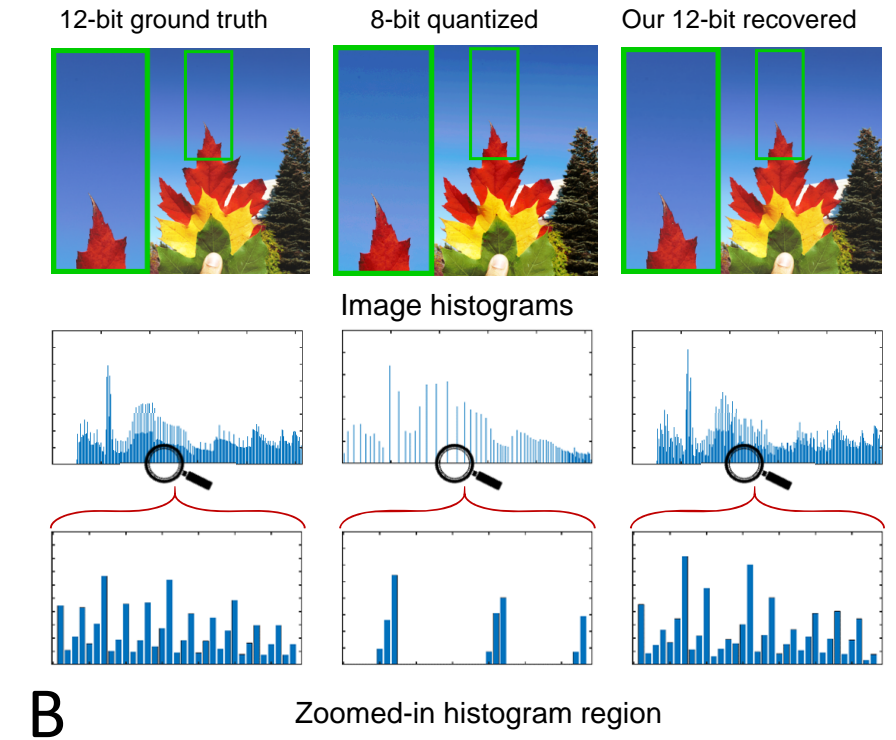


Fig. S5. (A) Shows a ground truth 12-bit HBD image, its 8-bit quantized LBD version, and our recovered 12-bit HBD result. The image has low contrast as shown by its image histogram. The green box denotes a zoomed-in region of the image. (B) Shows the same three images with histogram equalization applied. Due to its low bit depth, the 8-bit image has gaps in its histogram and exhibits visual banding. Our recovered 12-bit HBD image has a similar visual appearance and histogram profile as the ground truth 12-bit HBD image.